Structural investigations of Pt/TiO_x electrode stacks for ferroelectric thin film devices

Jiang-Li Cao,[a] Axel Solbach, and Uwe Klemradt
Physikalisches Institut B II, RWTH Aachen Universitat, Germany

Thomas Weirich and Joachim Mayer
Gemeinschaftslabor für Elektronenmikroskopie, RWTH Aachen Universitat, Germany

Herbert Horn-Solle
Lehrstuhl für Lasertechnik, RWTH Aachen Universitat, Germany

Ulrich Böttger, Peter J. Schorn, T. Schneller, and Rainer Waser
Institut für Werkstoffe der Elektrotechnik II, RWTH Aachen Universitat, Germany

(Received 24 September 2005; accepted 1 April 2006; published online 9 June 2006)

Effects of the thermal treatment and the fabrication process of $Pb(Zr_{0.3}Ti_{0.7})O_3$ (PZT) thin films using chemical solution deposition on Pt/TiO_x electrode stacks were investigated using complementary analytical techniques including atomic force microscopy (AFM), x-ray photoelectron spectroscopy, high-resolution transmission electron microscopy, and grazing incidence x-ray reflectivity of synchrotron radiation. The surface and interface structures of the Pt/TiO_x electrode stacks with different thermal treatments, and the $PZT/Pt/TiO_x$ sample were examined. The propagation of Pt hillocks on the bare Pt/TiO_x electrode stacks upon the annealing was observed. AFM observations also revealed that the upper surface of the Pt bottom electrode under PZT thin film became rougher than that of the bare Pt electrode with the same thermal history. Global structural information including the density, surface or interface root-mean-square roughness, and thickness of each constituent layer in the samples were determined using x-ray reflectivity. A density decrease of the Pt layer upon the annealing or during the fabrication of PZT thin films was found from fitting the specular reflectivity, and further confirmed by the negative shift of the Yoneda peak of Pt in the diffuse reflectivity. The formation of Pt hillocks on the bare Pt electrodes was attributed to the compressive stress during the high-temperature annealing caused by the limited incorporation of Ti and O into the Pt layer. Roughening of the PZT/Pt interface was ascribed to the interaction between the compressive stress in Pt and the indentation by the PZT crystallization and grain growth during the annealing. © *2006 American Institute of Physics*. [DOI: 10.1063/1.2202015]

I. INTRODUCTION

$Pb(Zr_x,Ti_{1-x})O_3$ (PZT) ferroelectric thin films have attracted much attention for their applications in the computer memory industries and microelectromechanical systems.[1,2] These devices have a typical planar capacitor structure with the ferroelectric layer sandwiched by a top electrode and a bottom electrode, normally integrated on a silicon substrate. In such a complex hybrid of stratified layers, the compatibility of the compositional layers and elements is a very important concern since they can all affect the performance and reliability of the final devices to a certain extent.[3]

Pt is regarded as a standard electrode material for the fabrication of PZT thin films owing to its compatibility with the integration process such as excellent oxidation resistance at high temperatures and high conductivity though the PZT capacitors with Pt electrodes show poor reliability, for example, electrical fatigue and imprint effect.[1,4] During the device fabrication, the electrodes need to withstand a series of thermal treatments in oxidizing atmosphere. Therefore, the high-temperature behavior of the electrodes is crucial for the performance and reliability of the devices. Previously, a thin intermediate layer of Ti was often introduced to improve the poor adhesion ability of Pt on SiO_2. However, the Pt/Ti metallic electrode shows poor thermal stability and reliability including the formation of Pt hillocks[5–8] or bumps under thermal conditions,[9] surface morphology evolution during aging,[7] short circuit of ferroelectric capacitors caused by the Pt hillocks,[10] severe diffusion of Ti into Pt, and even encapsulation of Pt hillocks with TiO_x during annealing.[6,9–11] In contrast, Sreenivas *et al.* reported that the Pt/TiO_x electrode structure shows an improved thermal stability.[6]

For a given ferroelectric medium with a certain chemistry and structure, the ferroelectricity is dependent on the electrical and mechanical boundary conditions to a great extent. As the whole multilayer is formed through a layer-by-layer deposition on the substrate from the bottom to the top, the lower layers will have certain influences on the upper layers. For example, by using Pt/TiO_2 electrodes with TiO_2 of random orientation, anatase and rutile structure, respectively, the ferroelectric thin films had different electrical

[a]Author to whom correspondence should be addressed; present address: School of M4, University of Nottingham, Nottingham NG7 2RD, UK; FAX: 00 44 (0)115 9513800; electronic mail: cao@physik.rwth-aachen.de

properties.[12] On the other hand, the fabrication process of the upper layers will definitely have some effects on the lower ones. Therefore, the properties of all the constituent layers in the hybrid devices need to be investigated thoroughly while their compatibility calls for intensive studies. However, so far the structural changes and element diffusions in the Pt/TiO_x electrode upon the thermal budget of the devices have not been well understood.

In the present study, comprehensive analytical techniques were used to investigate the effects of the thermal treatment and the fabrication process of PZT ceramic films on the Pt/TiO_x electrode stacks. The structure and surface composition of the Pt/TiO_x electrode stacks were examined by atomic force microscopy (AFM), x-ray photoelectron spectroscopy (XPS), and high-resolution transmission electron microscopy (HRTEM). The thickness, surface or interface roughness, and density of each constituent layer in the Pt/TiO_x electrodes with different heat treatments were characterized by grazing incidence x-ray specular and diffuse reflectivity of synchrotron radiation under nondestructive conditions.

II. EXPERIMENT

A. Sample preparation

Three Pt/TiO_x electrode stacks with different thermal treatments and a $Pb(Zr_{0.3}Ti_{0.7})O_3/Pt/TiO_x$ thin film sample were used in this study. Firstly, a silicon wafer with (100) orientation and a thickness of 0.6 mm was thermally oxidized to form a SiO_2 amorphous surface layer with a thickness of about 300 nm. Secondly, a Ti layer was sputtered as the adhesion layer at room temperature and subsequently oxidized at 700 °C for 5 min in oxygen. Hereafter, unless otherwise stated, all the annealing was performed in oxygen using a rapid thermal annealing (RTA) oven. Thirdly, a Pt layer of about 100 nm thick was deposited by dc sputtering on the TiO_x layer at 200 °C and subsequently crystallized at 700 °C for 5 min. Fourthly, the silicon wafer was cut into small pieces of 1×1 in.^{2}. Here, three pieces of electrode stacks were taken out from the batch for analyses. One of them was designated as *unannealed*. The other two were further annealed at 700 °C (the crystallization temperature of the ferroelectric films) for 3 and 10 min and were designated as 3 and 10 min *annealed*, respectively. For the preparation of the $Pb(Zr_{0.3}Ti_{0.7})O_3$ (PZT) thin film samples, a chemical solution deposition (CSD) process was used through spin coating on an unannealed Pt/TiO_x electrode stack.[13] After the deposition of a PZT layer, the sample was crystallized at 700 °C for 5 min and postannealed at 700 °C for 5 min. For the further examination of the buried Pt surface, the covering PZT film was removed through chemical etching using diluted hydrofluoric (HF) acid after the relevant examinations.

B. Analytical techniques

A Digital Instruments Dimension 3100 AFM was used in tapping mode to characterize the surface topography of the samples. XPS with Mg $K\alpha$ radiation was used to derive the chemical composition of the Pt electrode surface. The sampling depth was below 10 nm and the lateral area was about 8 mm^2. TEM investigations were performed using a Philips TECNAI FEI 20 with an energy filter (Gatan GIF 2000), an energy dispersion of x-ray (EDX) detector, and a high angle annular dark field (HAADF) detector. A thin TEM cross-sectional lamella with a thickness less than 100 nm was prepared by focused ion beam (FIB) cutting on a FEI STRATA FIB 205.

X-ray reflectivity (XRR) measurements were conducted on a high-resolution reflectometer at Deutsches Electronen Synchrotron (DESY) beamline E2 by using 11 keV monochromized x rays. For each sample, specular reflectivity scan ($\theta-2\theta$ scan), rocking scan ($\alpha_i+\alpha_f=$const), offset scan ($\alpha_i-\alpha_f=\pm2\varepsilon$), and detector scan ($\alpha_i=$const) were performed, where α_i is the incidence angle, α_f is the exit angle, and ε is the offset angle which was determined experimentally and just as big as to exclude the specular reflection. The beam had a height of 75 μm in the scattering plane and a horizontal width of 2 mm. The horizontal y direction of the slit before the detector was widely opened and the x direction was kept subtending an angle smaller than twice of the full width of half maximum (FWHM) of the rocking scan. For all the scans, dark currents were measured and deducted. The diffuse background calculated as the average of the two offset scans was subtracted from the raw specular reflectivity as well. The specular reflectivity was plotted as a function of the vertical momentum transfer $q_z=4\pi\sin\theta/\lambda$ (incidence angle equal to reflection angle), where q_z is the momentum transfer perpendicular to the sample surface, θ is the grazing incidence angle, and λ is the wavelength of the x rays. Illumination effect was corrected because a part of the beam passed over the sample in the low angle region. The fits to the specular reflectivity were performed using the Parratt algorithm[14] implanted into the PCTRF program[15] in which the surface or interface root-mean-square (rms) roughness, thickness, and density of each constituent layer were the fitting parameters. The roughness was treated as a small perturbation of a smooth surface or interface which is a Gaussian variable.

III. RESULTS

A. Surface and interface analyses

Figures 1(a) and 1(b) give the AFM surface images of the unannealed Pt/TiO_x electrode with different magnifications. Figures 1(c) and 1(d) show the AFM surface images of the 3 and 10 min annealed Pt/TiO_x electrode stacks, respectively. The Pt surfaces are continuous and dense with very fine grains. There are many minute hillocks on the surfaces of the three electrodes. In Fig. 1(b), it can be seen that most of the hillocks are located along the grain boundaries. Only few hillocks can be observed on the relative flat Pt grain facets, as indicated by the white arrow. With increasing annealing time the population and average size of these hillocks increase evidently. The Pt grains exhibit slight coarsening due to the further grain growth during the annealing, which is similar with the observation on Pt/Ti metallic bilayer electrode annealed in oxygen atmosphere.[10] The surface roughness values of the three electrodes are 1.1, 1.0, and

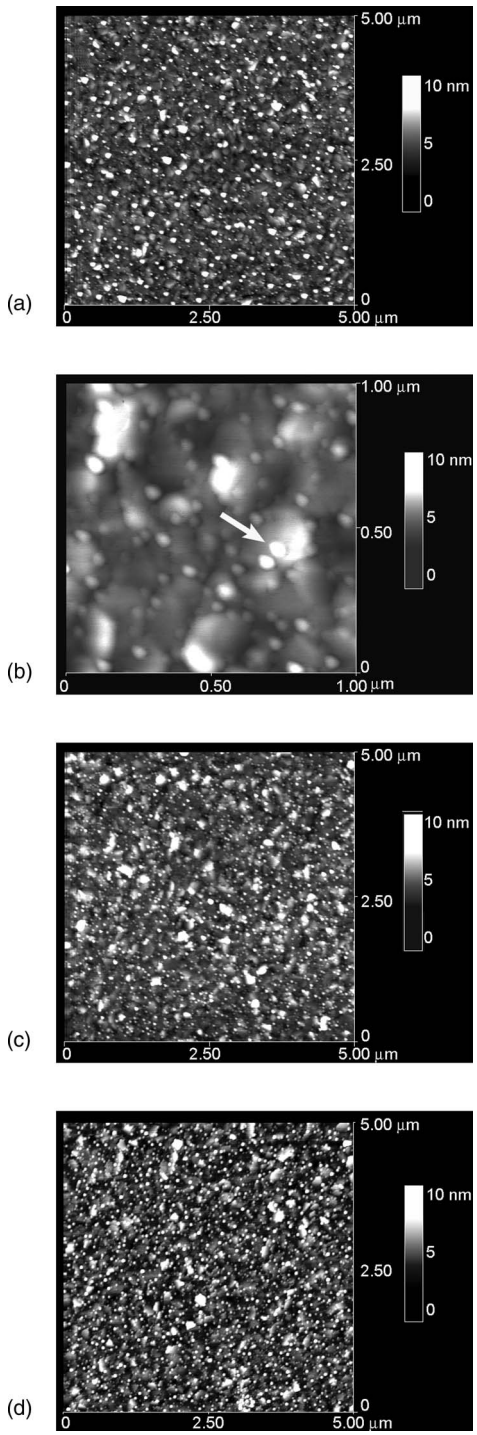

FIG. 1. AFM images of the Pt surface morphologies of the unannealed electrode (a) at low magnification and (b) high magnification, and (c) the 3 and (d) 10 min annealed electrodes.

1.2 nm, respectively. Though the surface morphology of the electrode changes significantly upon the annealing, the surface roughness change is negligible.

To determine the composition of the Pt surface and the hillocks especially, XPS surface analyses were conducted. The XPS spectra of the three Pt/TiO_x electrode stacks are plotted in Fig. 2, in which all the peaks are labeled with the corresponding elements. Only Pt and the impurity elements of C, O, and N are found, while the Ti signal is not observed. The results reveal that the electrode surfaces including the

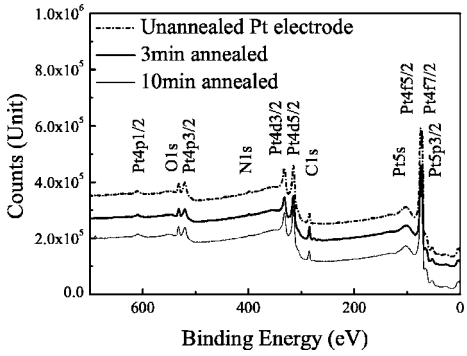

FIG. 2. XPS surface spectra of the unannealed, and 3 and 10 min annealed electrode stacks.

hillocks are constituted of Pt, while Ti is unable to penetrate up to the Pt surface during the 10 min annealing.

Figure 3(a) gives an AFM surface image of the PZT ceramic film sample. The PZT ceramic is very dense and consists of fine grains with a diameter of around 150 nm. Figure 3(b) shows an AFM surface image of the underlying Pt electrode with the covering PZT film being chemically removed. The surface roughness of this Pt electrode is 2.0 nm. This Pt electrode in the PZT thin film received 10 min of annealing in total, the same as the 10 min annealed Pt/TiO_x electrode stack. However, through the comparison between Figs. 1(d) and 3(b) it can be seen that the Pt surface becomes not only rougher, but also quite different from the 10 min annealed bare Pt surface. Some areas of the Pt surface, i.e., the previous PZT/Pt interface, have been indented by the PZT ceramic grains, as indicated by the two white arrows in the AFM image as an example. Additionally, the population of the small hillocks on the Pt surface de-

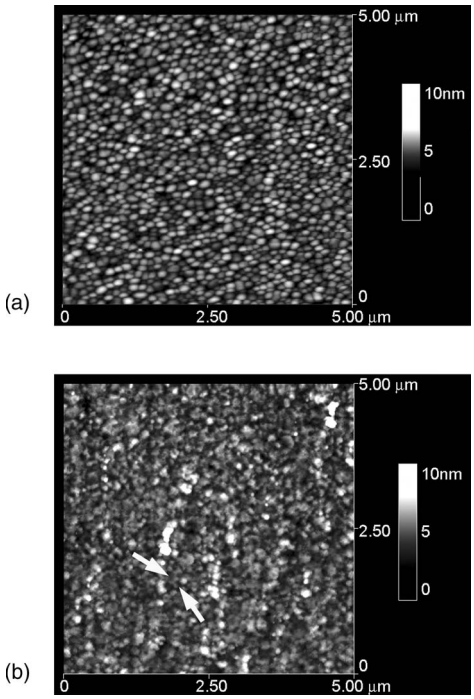

FIG. 3. AFM surface images of (a) the PZT ceramic film and (b) the Pt bottom electrode disclosed after the covering PZT ceramic was removed by chemical etching.

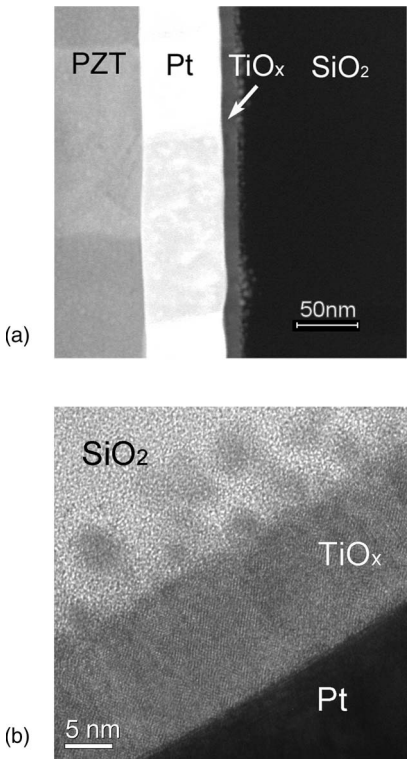

FIG. 4. (a) TEM cross-sectional high angle annular dark field image of the multilayer structure of the PZT thin film. From left to right: PZT, Pt, TiO_x, and SiO_2, respectively. (b) HRTEM image of the TiO_x layer, and the interfaces of Pt/TiO_x and TiO_x/SiO_2.

creases significantly. The drastic change of the Pt surface morphology during the film fabrication reveals that some new processes during the PZT crystallization, besides the thermal annealing itself, should be responsible for the changes.

The multilayered structure of the $PZT/Pt/TiO_x$ sample was examined using TEM. Figure 4(a) gives a cross-sectional HAADF image of the sample in which the atomic number contrast is clearly revealed. From left to right the layers are PZT ceramic, Pt electrode, TiO_x, and SiO_2, respectively. The interfaces of PZT/Pt and Pt/TiO_x are very clear, which indicates that the diffusion at these two interfaces is not strong. By contrast, there are many spots extending from TiO_x into SiO_2 at the interface of TiO_x/SiO_2, which reveals the diffusion of Pb and probably Ti as well into SiO_2.[16] Figure 4(b) shows a HRTEM image of the TiO_x/SiO_2 interface and the TiO_x layer. The TiO_x grains are randomly oriented in the plane. Through Fourier transformation to determine the d spacing, it is found that the TiO_x has a slight nonstoichiometric Ti:O ratio, deviating from TiO_2, and is constituted of oxygen-deficient components such as Ti_8O_{15} according to JCPDS File No. 85-1060. The shadowlike spots in the amorphous SiO_2 are indicative of the segregation of the diffused Pb and Ti.

B. X-ray specular reflectivity

X-ray specular and diffuse reflectivity measurements were conducted to examine the multilayered structure of the Pt/TiO_x electrode stacks with different thermal treatments.

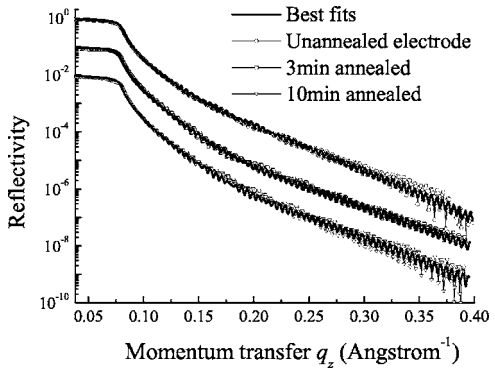

FIG. 5. Specular reflectivity of the unannealed, and 3 and 10 min annealed Pt/TiO_x electrode stacks. The best fits to the experimental specular reflectivity curves are also given (solid line).

With the use of highly intense and parallel x rays of synchrotron radiation, the reflected beam from deeper layers can be also recorded, and hence the structural analysis of buried layers becomes feasible under nondestructive conditions. X-ray specular reflectivity curves of these three samples are displayed in Fig. 5. For these three curves, the reflectivity intensity covers more than seven orders of magnitude. The reflectivity curves below the total external reflection angle of Pt are relatively flat because most of the beams are reflected and only the evanescent wave is scattered. Then the reflectivity decreases rapidly with increasing q_z beyond the Pt critical angle. The periodic oscillations from about 0.1 $Å^{-1}$ of q_z result from the interference of the reflected beams from the underlying interfaces with those from the Pt surface. Since the Pt layer has the highest electron density in the multilayered structure, the reflected beams from all the interfaces in the whole structure will contribute to the interference beyond the critical angle of Pt.

The experimental specular reflectivity data are fitted by the program PCTRF with Parrott algorithm, as shown also in Fig. 5 (solid lines). Note that here SiO_2 is used as the substrate because the x rays are not able to penetrate the SiO_2 layer with a thickness of 300 nm. For simplicity, Ti_8O_{15} is used for fitting the specular reflectivity in lieu of TiO_x. The roughness obtained from x-ray reflectivity characterizes the perpendicular electron density fluctuations or the electron density disorder at the surface or interfaces. For fitting these three reflectivity curves, it is found that the surface roughness cannot be described well within the simple Gaussian variable assumption. A low-density surface layer on top of the Pt layer must be introduced, which actually coincides with the AFM observation as have been observed that there are many tiny hillocks on the Pt surfaces. In essence, the structure model of low-density $Pt/Pt/TiO_x/SiO_2$ for fitting the specular reflectivity reflects the superposition of the very thin Pt-hillock layer on the bulk Pt layer. The structural characteristics of the three Pt/TiO_x electrode stacks are summarized in Table I together with error margins. The increase of the Pt surface layer density and thickness upon the annealing indicates qualitatively the increase of the population and size of the Pt hillocks. On the other hand, the mass density of the Pt bottom electrode decreases upon the annealing. The Pt/TiO_x interface roughness hardly changes, suggesting the

TABLE I. The thickness (d), density (ρ), and surface or interface roughness (σ) of the constituent layers in the unannealed, and 3 and 10 min annealed electrode stacks obtained from best fits of the specular reflectivity curves, assuming a stack of low-density $Pt/Pt/TiO_x$ of horizontally homogeneous layers on a SiO_2 substrate.

Constituent layers	Structure parameters	Unannealed	3 min annealed	10 min annealed
Surface Pt	σ(Å)	14.5±1	11.5±1	11.5±1
	ρ(g/cm^3)	9.1±0.3	12.7±0.3	13.5±0.3
	d(Å)	8.0±2	10±2	11±1
Pt	σ(Å)	6.2±0.2	5.5±0.2	6.0±0.2
	ρ(g/cm^3)	21.0±0.1	20.5±0.1	20.4±0.1
	d(Å)	1027±2	1003±2	1010±2
TiO_x	σ(Å)	12.0±3	13.0±3	13.0±3
	ρ(g/cm^3)	4.2±0.3	4.2±0.3	4.2±0.3
	d(Å)	192±2	185±2	198±2
SiO_2	σ(Å)	5.1±0.5	5.6±0.5	5.6±0.5
	ρ(g/cm^3)	2.2	2.2	2.2

absence of a strong diffusion at the interface during the annealing.

The PZT thin film sample was also examined using x-ray specular reflectivity (the detailed investigations can be found in a previous work).[16] As determined from fitting the reflectivity, the PZT/Pt interface roughness is 21.0 Å and the Pt density is 20.6 g/cm^3. It means that the density of the Pt bottom electrode decreased by 0.4 g/cm^3 during the PZT film fabrication. Additionally, the PZT/Pt interface roughness is greater than that of the 10 min annealed Pt electrode if we assume the sum of the surface layer thickness and the Pt/Pt interface roughness as the surface roughness of the Pt electrode. The increase of the Pt surface roughness also agrees with the AFM observation in Figs. 1(d) and 3(b). Here, it should be noted that it is unnecessary to assume the roughness from XRR and AFM to be equal because these two roughness values have different physical meanings. The rms roughness from XRR reveals the electron density fluctuation at the surface or interfaces seen by the x rays within a suitable model, while that from AFM is defined by the detectable morphological structural disorder of the surface.

C. X-ray diffuse reflectivity

Figure 6 gives the detector scans of the three Pt/TiO_x electrode stacks in which the sample was fixed while the detector was rotated. In these three curves, the first peak from the left is the Yoneda peak of Pt, while the second peak is the specular reflection. Accordingly, the critical angles of Pt of the unannealed, 3 and 10 min annealed electrode stacks are determined to be 0.401±0.002°, 0.394±0.002°, and 0.390±0.002°. As determined previously, the critical angles of PZT and Pt in the PZT thin film are 0.221±0.003° and 0.397±0.001°.[16] The decrease of the Pt critical angle means the density decrease of the Pt layer during the thermal treatment, which confirms the specular reflectivity results. The vertical roughness correlation was not established during the sample preparation because of the absence of periodic oscillations.

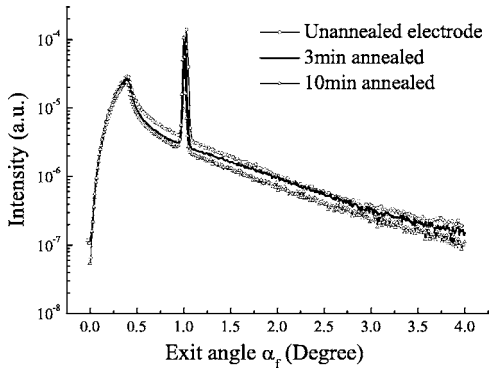

FIG. 6. Detector scans of the unannealed, and 3 and 10 min annealed Pt/TiO_x electrode stacks with the incidence angle at 1.03°, 1.01°, and 1°, respectively, from which the critical angles of Pt are determined.

IV. DISCUSSION

A. Formation of Pt hillocks on the bare Pt electrode

Minute Pt hillocks are observed on the Pt/TiO_x electrode stacks. The hillocks are determined to consist of Pt through the XPS analyses. The reported penetration of underlying Ti to the upper surface of Pt (Refs. 6 and 17) is not the case for the Pt/TiO_x electrode stacks investigated in this study. The Pt hillocks with radii typically ranging from 20 to 70 nm for the case at hand are much smaller than those on Pt/Ti electrode stacks as reported earlier.[8–10]

For Pt films deposited using dc sputtering at low temperatures, a compressive stress is generally present.[10,18–20] The stress is relaxed under high-temperature treatments through the formation of Pt hillocks and becomes tensile upon cooling down to room temperature because of the thermal strain.[8,19,20] That is the case for the unannealed Pt/TiO_x electrode in the present study. However, the population and size of the Pt hillocks increase upon the further thermal annealing, which strongly suggests the generation of a compressive stress during the annealing. In addition, it is found that the density of the Pt bottom electrode deceases upon the annealing. Previously, a similar but much stronger density decrease of the Pt layer in Pt/Ti bilayer electrode upon the annealing was reported and attributed to the strong diffusion of Ti and its following oxidation.[21,22] Though the diffusion at the Pt/TiO_x interface was not strong[6,11] or even undetectable as reported,[18] the limited diffusion and incorporation of Ti and O into Pt have been observed previously[23–26] and confirmed by scanning transmission electron microscopy.[16] Ti and O can migrate along the grain boundaries of Pt when the sample is annealed.[26] Therefore, here the slight density decrease of Pt is proposed to be induced by the limited incorporation of the light elements of Ti and O from the environments or neighboring layers. Meanwhile, a compressive stress is generated by the limited incorporation of Ti and O during the annealing. Under the compressive stress, Pt hillocks on the Pt electrode surface are formed mainly along the grain boundaries, as observed in Fig. 1(b).

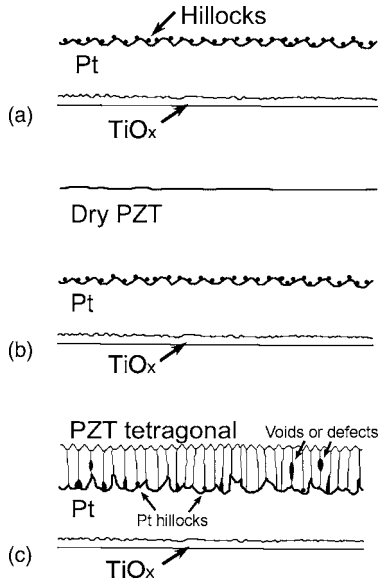

FIG. 7. Interpretation model for the roughening of the PZT/Pt interface during the PZT film fabrication. (a) A crystallized Pt/TiO_x electrode stack with many Pt hillocks on the surface, (b) the crystallized Pt/TiO_x electrode stack with a layer of dry PZT gel after the spin coating of a PZT layer and drying, and (c) the $PZT/Pt/TiO_x$ structure at low temperature with a rougher PZT/Pt interface after cooling down from high-temperature crystallization. A small amount of Pt hillocks remain on the Pt electrode, while some defects or voids may be present in the ceramic layer.

B. Roughening of the PZT/Pt interface

With the same thermal history, however, the Pt electrode underneath the PZT film has a quite different surface morphology from that of the bare Pt electrode, as shown in Figs. 1(d) and 3(b). The upper surface of the Pt electrode in a PZT film sample is rougher than that of the 10 min annealed bare Pt electrode according to the AFM observations. This evident increase of the Pt surface roughness agrees well with the XRR results. Furthermore, there are many indentations on the Pt layer while a small amount of Pt hillocks still remains, which indicates that the PZT grain growth in these areas may not be sufficient.

The roughening of the PZT/Pt interface should be attributed to the interaction between the PZT layer and Pt electrode during the PZT film fabrication. An interpretation model for the morphology evolution of the PZT/Pt interface is proposed, as illustrated in Fig. 7. Figure 7(a) gives a schematic drawing of an unannealed Pt/TiO_x electrode stack with many hillocks on the Pt surface. By the CSD method, a thin liquid layer is spin coated on the Pt/TiO_x electrode stack. After drying, hydrolysis, and pyrolysis of the organic ligands, the resulting film becomes amorphous or nanocrystalline, as shown in Fig. 7(b). Upon the crystallization treatment at 700 °C, the PZT film is crystallized and grain growth starts, following a nucleation-and-growth process, which is typical for CSD preparation of PZT films.[27] The CSD-derived PZT ceramic films in the present study display a columnar grain structure, which suggests that the nucleation occurs only on the substrate surface, but not in the films. Due to the growth of the columnar PZT grains, the relatively soft Pt surface is intruded. This answers for the indentations on the Pt surface, as observed in Fig. 3(b). Consequently, the Pt hillocks population decrease significantly. Meanwhile, some areas of the Pt surface are pushed up, as indicated in Fig. 7(c) as the black bumps underneath the PZT film, by the compressive stress from the indentation of the PZT grains and the incorporation of the elements from the neighboring layers.[16] This interaction should be responsible for the PZT/Pt interface roughening during the PZT film fabrication. Thus, the two aspects of PZT/Pt interface morphology change including the PZT/Pt interface roughening and the indentation formation can be interpreted.

V. CONCLUSIONS

The formation of the minute Pt hillocks on the Pt bottom electrode upon the thermal annealing is observed and attributed to the relief of the compressive stress in the Pt layer during the thermal treatment. For fitting the specular reflectivity of the electrode stacks, a structure model of low-density $Pt/Pt/TiO_x/SiO_2$ needs to be used to describe the Pt hillocks on top of the Pt electrode. With increasing annealing time the population and size of the Pt hillocks increase. However, the Pt surface roughness remains nearly unchanged according to the AFM and XRR measurements. The roughening of the PZT/Pt interface during the PZT film fabrication is attributed to the interaction between the PZT film and Pt electrode and an interpretation model is proposed.

The present investigation shows the evidence for the relatively stable Pt/TiO_x electrode structure in oxidizing atmosphere. XPS analyses indicate the absence of Ti on the Pt surface even after 10 min of oxygen annealing at 700 °C. However, the detailed investigation using x-ray specular and diffuse reflectivity reveals the density decrease of the Pt layer, which is proposed to be caused by the limited incorporation of light elements including Ti and O.

ACKNOWLEDGMENTS

One of the authors (J. L. C.) thanks Alexander von Humboldt Foundation for support to this Humboldt project. The authors are grateful to DESY for the project grant No. II-03-009. The authors thank M. Wuttig for the AFM observations.

[1] J. F. Scott and C. A. Paz de Araujo, Science **246**, 1400 (1989).
[2] O. Auciello, J. F. Scott, and R. Ramesh, Phys. Today **51**(7), 22 (1998).
[3] J. F. Scott, Aust. J. Phys. **52**, 903 (1999).
[4] W. Warren, B. Tuttle, D. Dimos, G. Pike, H. Al-Shareef, R. Ramesh, and J. Evans, Jpn. J. Appl. Phys., Part 1 **35**, 1521 (1996).
[5] P. D. Hren, H. Al-Shareef, S. H. Rou, A. I. Kingon, P. Buaud, and E. A. Irene, Mater. Res. Soc. Symp. Proc. **260**, 575 (1992).
[6] K. Sreenivas, I. Reaney, T. Maeder, N. Setter, C. Jagadish, and R. G. Elliman, J. Appl. Phys. **75**, 232 (1994).
[7] G. A. C. M. Spierings, G. J. M. Dormans, W. G. J. Moors, M. J. E. Ulenaers, and P. K. Larsen, J. Appl. Phys. **78**, 1926 (1995).
[8] W. W. Jung, S. K. Choi, S. Y. Kweon, and S. J. Yeom, Appl. Phys. Lett. **83**, 2160 (2003).
[9] J. O. Olowolafe, R. E. Jones, A. C. Campbell, R. I. Hegde, C. J. Mogab, and R. B. Gregory, J. Appl. Phys. **73**, 1764 (1993).
[10] H. N. Al-Shareef and A. Kingon, in *Ferroelectric Thin Films: Synthesis and Basic Properties*, edited by C. P. de Araujo, J. F. Scott, and G. W. Taylor (Gordon and Breach, Amsterdam, 1996).
[11] T. Maeder, L. Sagalowicz, and P. Muralt, Jpn. J. Appl. Phys., Part 1 **37**, 2007 (1998).
[12] S. Okamura, N. Abe, Y. Otani, and T. Shiosaki, Integr. Ferroelectr. **52**, 127 (2003).
[13] C. Kugeler, P. Gerber, U. Bottger, and R. Waser, Integr. Ferroelectr. **54**,

527 (2003).
[14]L. G. Parratt, Phys. Rev. **95**, 359 (1954).
[15]U. Klemradt, PCTRF Multilayer Reflectivity Fitting Program (available on request).
[16]J. L. Cao *et al.*, J. Am. Ceram. Soc. **89**, 1321 (2006).
[17]N. Abe, Y. Otani, M. Miyake, M. Kurita, H. Takeda, S. Okamura, and T. Shiosaki, Jpn. J. Appl. Phys., Part 1 **42**, 2791 (2003).
[18]S. Y. Kweon, S. K. Choi, S. J. Yeom, and J. S. Roh, Jpn. J. Appl. Phys., Part 1 **40**, 5850 (2001).
[19]Y. Matsui, M. Hiratani, Y. Kumagai, H. Miura, and Y. Fujisaki, Jpn. J. Appl. Phys., Part 2 **37**, L465 (1998).
[20]K. Nakamura, Y. Otani, M. Kurita, S. Okamura, and T. Shiosaki, Jpn. J. Appl. Phys., Part 2 **44**, 8096 (2005).
[21]A. Ehrlich, U. Weiss, W. Hoyer, and T. Gessner, Thin Solid Films **300**, 122 (1997).
[22]M. Aspelmeyer, U. Klemradt, W. Hartner, H. Bachhofer, and G. Schindler, J. Phys. D **34**, A173 (2001).
[23]M. Alguero, M. L. Calzada, M. J. Martin, and L. Pardo, J. Phys. Chem. Solids **63**, 471 (2002).
[24]R. Schmiedl *et al.*, Appl. Phys. A: Mater. Sci. Process. **62**, 223 (1996).
[25]Y. M. Sun, D. N. Belton, and J. M. White, J. Phys. Chem. **90**, 5178 (1986).
[26]C. M. Greenlief, J. M. White, C. S. Ko, and R. J. Gorte, J. Phys. Chem. **89**, 5025 (1985).
[27]R. W. Schwartz, Chem. Mater. **9**, 2325 (1997).